第 33 卷第 1 期
2014 年 2 月

红外与毫米波学报
J. Infrared Millim. Waves

Vol. 33, No. 1
February, 2014

文章编号: 1001 -9014(2014)01 -0050 -05 DOI: 10. 3724/SP. J. 1010. 2014. 00050

Infrared detectors with high fill-factor absorber and low offset low noise readout circuit

HUANG Zhuo-Lei[1], WANG Wei-Bing[1,2,*], JIANG Wen-Jing[1,2], OU Wen[1,2], MING An-Jie[1,2], LIU Zhan-Feng[1,2], CHEN Da-Peng[1,2]

(1. Key Laboratory of Microelectronics Devices & Integrated Technology, Institute of Microelectronics, Chinese Academy of Sciences, Beijing 100029, China;
2. Smart Integrated Sensor Engineering Center, JiangSu Research and Development Center for Internet of Things, Wuxi 214135, China)

Abstract: By using infrared detector and readout circuit, an uncooled infrared detecting system was developed. The detector using diode as the temperature sensor is compatible with integrated circuit process. A new device structure was used to improve the fill-factor from 20% to 80%. The area of micromachined structure is 35 μm × 35 μm. The offset voltage of the readout circuit is 3 μV. The output noise of the detector is 2 μV. The responsivity of the detector is 7 894. 7 V/W, specific detectivity of the detector is 1.56×10^9 cmHz$^{1/2}$/W, noise equivalent temperature difference of the detector is 330 mK, and response time of the detector is 27 ms.

Key words: infrared detector; diode; fill-factor; absorber; readout circuit
PACS: 07. 57. Kp

一种具有高填充因子吸收层和低失调低噪声读出电路的红外探测系统

黄卓磊[1], 王玮冰[1,2*], 蒋文静[1,2], 欧 文[1,2], 明安杰[1,2], 刘战锋[1,2], 陈大鹏[1,2]

(1. 中国科学院微电子研究所微电子器件与集成技术重点实验室,北京 100029;
2. 江苏物联网研究发展中心智能集成传感器工程中心,江苏 无锡 214135)

摘要: 使用红外探测器及读出电路, 研制成功非制冷红外探测系统. 探测器用二极管作为温度传感器, 使其与集成电路工艺相兼容. 采用了新的器件结构, 使得填充因子从 20% 提高到 80%. 器件的微机械结构面积为 35 μm × 35 μm. 读出电路的失调电压为 3 μV. 探测器的输出噪声为 2 μV. 探测器的电压响应率为 7 894. 7 V/W, 黑体探测率 D * 为 1.56×10^9 cmHz$^{1/2}$/W, 噪声等效温差为 330 mK, 响应时间为 27 ms.

关 键 词: 红外探测器;二极管;填充因子;吸收层;读出电路
中图分类号: TN4 **文献标识码**: A

Introduction

Infrared detection technology has been widely used in many fields, such as military, industry, agriculture, medical treatment and so on. There are two kinds of infrared detector: cooled detector and uncooled detector. The cooled infrared detector converts infrared signal to electrical signal by photoelectric

Received date: 2013 - 01 - 10, **revised date**: 2013 - 10 - 20 **收稿日期**: 2013 - 01 - 10, **修回日期**: 2013 - 10 - 20
Foundation items: Supported by National Scie:nce and Technology Major Project of the Ministry of Science and Technology of China (2011ZX02507-004)
Biography: HUANG Zhuo-Lei(1985-), male, Nanning, doctor. Research area involves MEMS design and integrated circuit design. E-mail: huangzhuolei@ ime. ac. cn.
* **Corresponding author**: E-mail: wangweibing@ ime. ac. cn.

effect, and works at a low temperature. The uncooled infrared detector absorbs infrared radiation, and the infrared radiation will increase the temperature of the detector's absorber. The sensitive components in the detector will convert the change of temperature to electrical signal.

There have been many studies on uncooled infrared detector in recent years, since uncooled infrared detector is much superior in size, cost and power consumption compared with cooled infrared detector[1]. However the performance of the uncooled infrared detector is worse than the cooled one, which means that uncooled infrared detector needs other methods, such as new structure and high performance circuit to enhance its ability[2]. Although many approaches have been proposed for uncooled infrared detector, most of them are not compatible with integrated circuit process. In this paper we use diode as the temperature sensor, which is compatible with integrated circuit process. We will present the high fill-factor absorber and the low offset low noise readout circuit. Those are used to improve the performance of the detector.

1 Diode temperature sensor

In general, the relation between current density and terminal voltage of diode can be expressed by[3]:

$$J = J_s \exp\left(\frac{qV}{K_0 T}\right) \quad , \quad (1)$$

where J_s is the saturation current, q is the magnitude of electronic charge, K_0 is the Boltzmann's constant and T is the temperature of diode. The inverse function of equation(1) is:

$$V = \frac{K_0 T}{q} \ln \frac{J}{J_s} \quad . \quad (2)$$

After derivation, the temperature sensitivity of voltage can be expressed by:

$$\frac{dV}{dT} = \frac{V}{T} - \frac{(3 + \gamma/2)K_0}{q} - \frac{E_g}{qT} \quad , \quad (3)$$

E_g is the forbidden band width of Silicon, its value is 1.119 eV when T is 300 K. It can be assumed that the terminal voltage of diode is 0.8 V. The value of the temperature sensitivity can be calculated by equation (3), which is −1.32 mV/K.

The temperature of the detector will increase after absorbing the infrared radiation. The terminal voltage of diode will decrease when the temperature increases. Hence the higher fill-factor, the better performance of the detector[4]. Fig. 1[5] shows the structure of the diode temperature sensor with conventional absorber. The diode temperature sensor is supported by two legs including electrical interconnections. The infrared radiation absorber is directly on the diode, and filled with the dielectric film that is a thickness of 1/4 infrared wavelength between absorber and reflector. Although the process of this structure is simple, the infrared absorbing area is small and the fill-factor is only 20%.

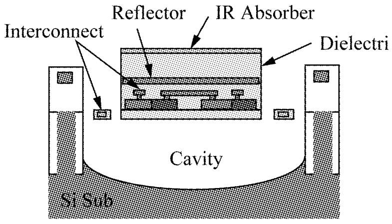

Fig. 1 The structure of diode temperature sensor with conventional absorber
图 1 具有传统吸收层结构的二极管温度传感器

To obtain higher sensitivity, the thermal conductance of support leg is designed to be as small as possible and the infrared absorbing area is designed to be as big as possible. Fig. 2 shows the structure of the diode temperature sensor with high fill-factor absorber. Compared with the conventional one, the dielectric film of the improved structure has been replaced by a vacuum gap with the same thickness, and the absorber is supported by two pillars. Thus the infrared absorbing area can be expanded to the whole device, and the fill-factor reaches 80%.

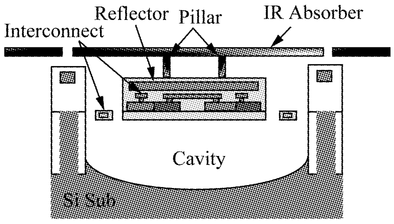

Fig. 2 The structure of diode temperature sensor with high fill-factor absorber
图 2 具有高填充因子吸收层结构的二极管温度传感器

The absorber can improve the responsivity by absorbing more infrared radiation. Meanwhile, it deteriorates the response time. In Fig. 1 the thermal conductance of dielectric film is very large compared with the thermal conductance of the support leg, and the thermal response time from the absorbing structure to the sensing structure is negligible. Hence the thermal response time can be expressed by:

$$\tau_1 = \frac{C_t}{G_t} \quad , \quad (4)$$

where C_t is the heat capacitance of the whole detector, G_t is the thermal conductance to the substrate. In Fig. 2 the thermal conductance of the pillars should be designed to be much larger than the thermal conductance of the support leg. So that the thermal response time from the absorbing structure to the sensing structure could be ignored, and the thermal response time can be expressed by:

$$\tau_2 = \frac{C_{ab} + C_{se}}{G_{leg}} \quad , \quad (5)$$

where C_{ab} is the heat capacitance of the absorbing structure, C_{se} is the heat capacitance of the sensing structure containing diodes, and G_{leg} is the thermal conductance of the support legs.

2 Chopper readout circuit

The suggested infrared detecting system has been implemented as shown in the block diagram of Fig. 3. The system consists of an absorber, a diode temperature sensor and a readout circuit. The output voltage of the diode temperature sensor is small. The magnitude of the output voltage is microvolt or lower. Hence it needs a readout circuit to amplify the weak signal for later processing, such as analog to digital converting. However conventional integrated amplifiers are known for their high 1/f noise and offset[6]. Noise will reduce the noise equivalent temperature difference (NETD), and offset will reduce the dynamic range of the detector. Hence chopper technology is introduced to the readout circuit to reduce the 1/f noise and offset.

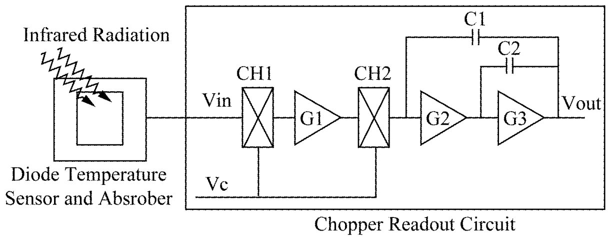

Fig. 3 Infrared detecting system block diagram
图3 红外探测系统结构图

In Fig. 3, CH1 and CH2 are modulators. G1, G2 and G3 are transconductors. C1 and C2 are compensation capacitors. Vc is the chopper signal. The output signal of sensor is transposed to a higher frequency where there is no 1/f noise by the modulator CH1, and then demodulated back to the baseband after amplification by modulator CH2. Most 1/f noise and offset are modulated to the chopper frequency by modulator CH2, and then filtered out by a low-pass filter. The low-pass filter consists of G2, G3, C1 and C2.

The input noise of the readout circuit can be expressed as[7]:

$$S_{Nin} = S_{N0}\left(1 + \frac{f_k}{|f|}\right) \quad , \quad (6)$$

S_{N0} is the white noise, and f_k is the corner frequency. After chopped by the CH2, the output noise becomes:

$$S_N = A^2 S_{N0}\left(1 + \frac{17f_k}{2\pi^2 f_{chop}}\right) \quad , \quad (7)$$

A is the gain of G1 and f_{chop} is the chopper frequency. Since the CH2 is followed by a low-pass filter, the output noise spectrum of the readout circuit can be expressed by:

$$S_N = A^2 S_{N0}\left(1 + \frac{17f_k}{2\pi^2 f_{chop}}\right)\left(\frac{1}{1 + 2\pi RCf}\right) \quad , \quad (8)$$

R is the output resistance of G1, and C is the value of C1. The residual offset after chopper is[8]:

$$V_{off} = A\frac{2\pi}{T}V_{inj} \quad , \quad (9)$$

V_{inj} is charge injection of modulator and T is the period of the chopper signal. The low-pass filter removes all but the first harmonic of the chopped offset voltage. The residual offset is then equal to:

$$V_{off} = 4AV_{inj}\left(\frac{2\pi}{T}\right)^2 \quad . \quad (10)$$

3 Experimental results

Figure 4 is the photo of high fill-factor absorber, and Fig. 5 is the photo of chopper readout circuit. Test results show that the proposed detector's performance is better than the detector without high fill-factor absorber and chopper readout circuit. The performance of the detector with high fill-factor absorber is better than the detector with conventional absorber as shown later. The test performances of detectors were compared in two cases, such as only single device and the entire system including readout circuit. The performance of the infrared detector with high fill-factor and low offset low noise readout circuit is presented below.

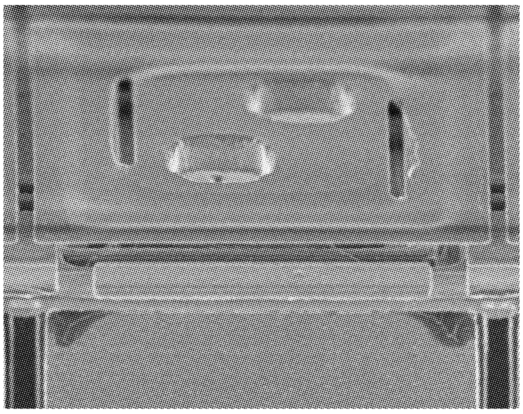

Fig. 4 Absorber
图 4 吸收层

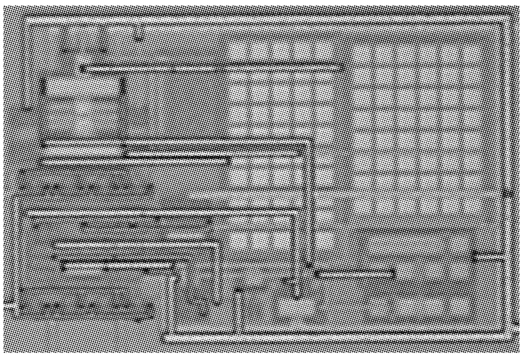

Fig. 5 Readout circuit
图 5 读出电路

The performance of the detector can be judged by specific detectivity, which is defined as[9]:

$$D^* = \frac{R}{V_{noise}} \sqrt{A \cdot \Delta f} \quad , \quad (11)$$

R is the response sensitivity, V_{noise} is the noise voltage, A is the area of device, and Δf is the measured bandwith. The ratio of generated voltage to received power stands for the detector's response sensitivity:

$$R = \frac{V}{P} \quad . \quad (12)$$

The response sensitivity and the noise voltage of the diode sensor with conventional absorber and proposed absorber were measured respectively. The specific detectivity of diode sensor with conventional absorber is 4.68×10^6 cmHz$^{1/2}$/W. The specific detectivity of diode sensor with high fill-factor absorber is 2.07×10^7 cmHz$^{1/2}$/W, which is 4.4 times greater than the former one. The response sensitivity and noise voltage of detector with high fill-factor and readout circuit were measured too. Its specific detectivity is 1.56×10^9 cmHz$^{1/2}$/W, which is 75 times greater than the detector without readout circuit. The test results of the three detectors are shown in table 1. Type I is conventional absorber without readout circuit. Type II is high fill-factor absorber without readout circuit. Type III is high fill-factor absorber with readout circuit.

Table 1 specific detectivity of three detectors
表 1 三种探测器的黑体探测率

	Type I	Type II	Type III
D^* (cmHz$^{1/2}$/W)	4.68×10^6	2.07×10^7	1.56×10^9

Figure 6 shows the offset voltage at different frequencies of the readout circuit. At first the offset voltage decreases as chopping frequency increases because of the low-pass filter, then the offset voltage increases as chopping frequency increases because of charge injection. There is a lowest offset voltage, which is 3 μV. Fig. 7 is the large signal transient response of the readout circuit, which shows that the dynamic range of the readout circuit can reach 4.7 V.

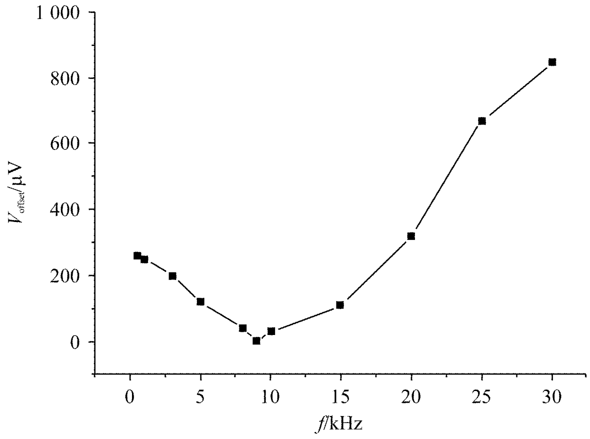

Fig. 6 Offset voltage of readout circuit
图 6 读出电路的失调电压

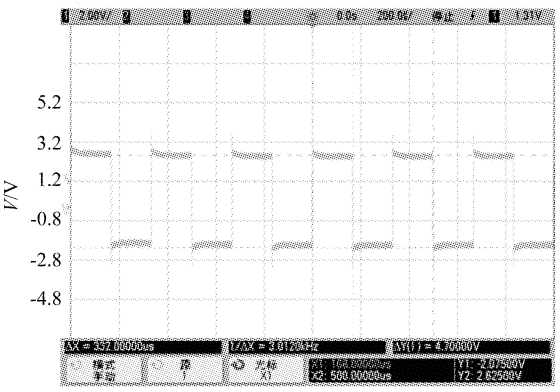

Fig. 7 Large signal response of readout circuit
图7 读出电路的大信号响应

The output noise of the infrared detector with high fill-factor absorber and low offset low noise readout circuit is about 2 μV, which is shown in Fig. 8. The transient response of the infrared detector with high fill-factor absorber and low offset low noise readout circuit is shown in Fig. 9, which shows that the response time of the detector is 27 ms. Table 2 compares this work to other infrared detectors in references.

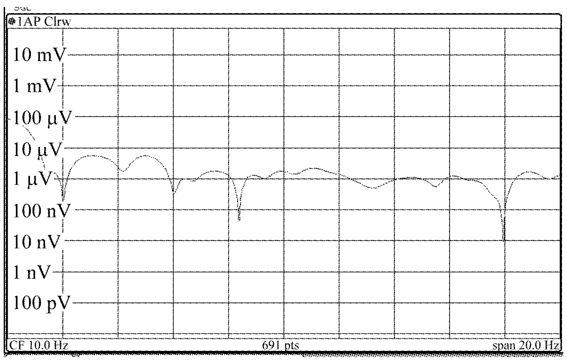

Fig. 8 Output noise of the detector
图8 探测器的输出噪声

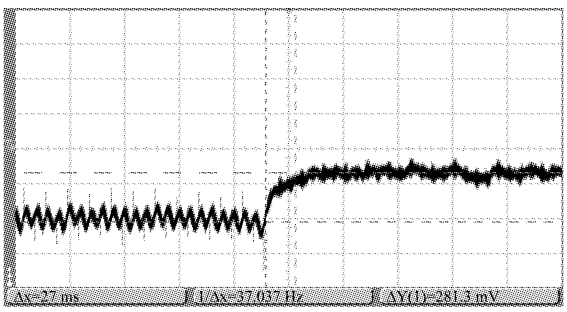

Fig. 9 Transient response of the detector
图9 探测器的瞬态响应

Table 2 Main performance of the proposed infrared detector and its comparison
表2 推荐的红外探测器与参考文献中红外探测器的性能对比

	Responsivity	Detectivity	Response time
	(V/W)	($cmHz^{1/2}/W$)	(ms)
[5]	4970	9.7×10^8	36
[10]	5700	1.2×10^8	7
[11]	34.7	1.93×10^7	6.2
This work	7894.7	1.56×10^9	27

4 Conclusion

An infrared detector with high fill-factor absorber and low offset low noise readout circuit is presented. The structure of the absorber and the readout circuit are shown. The diode is used as the temperature sensor, which is compatible with integrated circuit process. The designed infrared detector exhibit responsivity of 7 894.7 V/W, specific detectivity of 1.56×10^9 $cmHz^{1/2}/W$, noise equivalent temperature difference of 330 mK, and response time of 27 ms.

REFERENCES

[1] Roncaglia A, Mancarella P, Cardinali C C, CMOS-compatible fabrication of thermopiles with high sensitivity in the 3-5 μm atmospheric window [J], *Sensors and Actuators B*, 2007, **125**(1), 214-223.
[2] Ueno M, Kosasamaya Y, Sugina T, *et al*. 640×480 pixel uncooled infrared FPA with SOI diode detectors[J], *Proc. SPIE-Infrared Technology Applications XXXI*, 2005, 5783: 566-577.
[3] Sze S M. Physics of Semiconductor Devices [M]. New York: John Wiley & Sons, 1981.
[4] Kimata M, Ueno M, Takeda M, *et al*. SOI diode uncooled infrared focal plane arrays[J]. *Proc. SPIE-Quantum Sensing and Nanophotonic Devices III*, 2006, 6172: 6120x. 1-6120x. 11.
[5] Eminoglu S, Tanrikulu M, Akin T, A low-cost 128×128 uncooled infrared detector array in CMOS process [J], *Journal of microelectromechanical system*, 2008, **17**(1): 20-30.
[6] Enz C, Temes G C. Circuit techniques for reducing the effects of op-amp imperfections: autozeroing, correlated double sampling, and chopper stabilization[J]. *Proceedings of IEEE*, 1996. 1584-1614.
[7] Enz C, Vittoz E A, Krummenacher F. A CMOS chopper amplifier [J]. *IEEE J Solid-State Circuits*, 1987, 22: 335-342.
[8] Menolfi C, Huang Qiu-Ting A low-noise CMOS instrumentation amplifier for thermoelectric infrared detectors [J], *IEEE J Solid-State Circuit*, 1997, 32: 968-976.

(下转第67页)

waveguide circuit is presented. With the knowledge of the operating frequency and beam voltage, we can obtain the initial structural parameters of the FWTWT. An optimized structure of 220 GHz folded waveguide slow-wave structure was designed in order to tradeoff the bandwidth and gain. Cold characteristics of a folded waveguide circuit including dispersion relation and interaction impedance were calculated using HFSS. The simulative values have good agreement with the theory ones. The large signal performance was predicted by PIC code. The nonlinear simulation shows that gain is 13.5 dB at 220 GHz, and 3 dB bandwidth of 11 GHz (213 ~ 224 GHz). The micromachined process of the folded waveguide circuit has been discussed. The first example of folded waveguide circuits was fabricated by UV-LIGA. Optimization of the UV-LIGA processing to achieve the desired dimensional tolerances was discussed. In order to eliminate regenerative oscillations, attenuator for a folded waveguide TWT is important. In THz TWT, the traditional BeO attenuator isn't fabricated because of its size. DRIE-machined Si attenuator shows promise as drop-in components for THz TWT. The design and DRIE fabrication of Si attenuator is in progress.

REFERENCES

[1] Booske J H, Kory C L, Gallagher D, *et al.* Terahertz-regime, micro-VEDs: evaluation of micromachined TWT conceptual designs[C]. IEEE PPPS2001, USA: Las Vegas, 2001: 17 – 22.

[2] Ives R L. Microfabrication of high frequency vacuum electron devices[J]. *IEEE Trans. Plasma Sci*, 2004, **32**(3): 1277 – 1291.

[3] Han S T, Jeon S G, Shin Y M, *et al.* Experimental investigations on miniaturized high-frequency vacuum electron devices[J]. *IEEE Trans. Plasma Sci*, 2005, **33**(2): 679 – 684.

[4] Song J J, Decarlo F, Kang Y W, *et al.* MM-wave cavity/klystron developments using deep x-ray lithography at the advanced photon source[C]. APAC1998, Japan: Tsukuba, 1998: 298 – 300.

[5] Han S T, So J K, Jang K H, *et al.* Investigations on a microfabricated FWTWT oscillator[J]. *IEEE Trans.* Electron Devices, 2004, **52**(5): 702 – 708.

[6] Kory C L, Dayton J A, Mearini G T, *et al.* 95 GHz helical TWT design [C]. IVEC2008, USA: Monterey, 2008: 125 –126.

[7] Shin Y M, Park G S, Scheitrum G P, *et al.* Novel coupled-cavity TWT structure using two step LIGA fabrication[J]. *IEEE Trans. Plasma Sci*, 2003, **31**(6): 1317 – 1324.

[8] Feng Jin-Jun, Hu Yin-Fu, Cai Jun, *et al.* Progress of W-band 10W CW TWT[C]. IVEC2010, USA: Monterey, 2010: 501 – 502.

[9] Tucek J, Basten M, Gallagher D, *et al.* 220 GHz folded waveguide circuits for high power amplifiers [C]. IVEC2009, Italy: Rome, 2009: 108 – 109.

[10] He Jun, Wei Yan-Yu, Gong Yu-Bin, *et al.* Linear analysis of a W band groove-loaded folded waveguide traveling wave tube[J]. *PHYSICS OF PLASMAS*, 2010, **17**(11): 113305.

[11] He Jun, Wei Yan-Yu, Gong Yu-Bin, *et al.* Investigation on a W band ridge-loaded folded waveguide TWT[J]. *IEEE Trans. Plasma Sci*, 2011, **39**(8): 1660 – 1664.

[12] Gong Yu-Bin, Yin Hai-Rong, Yue Ling-Na, *et al.* A 140-GHz two-beam overmoded folded-waveguide Traveling-Wave Tube[J]. *IEEE Trans. Plasma Sci*, 2011, **39**(3): 847 – 851.

[13] Liu Sheng-Gang, Li Hong-Fu, Wang Wen-Xiang, *et al.* Introduction to microwave electronics[M]. Beijing: National defense industry press, 1985: 413 – 415.

[14] Han S T, Kim J I, Park G S. Design of a folded waveguide traveling-wave tube[J]. *Microw Opt Tech Lett*, 2003, **38**(2), 161 – 165.

[15] Dohler G, Gagne D, Gallagher D, *et al.* Serpentine waveguide TWT [C]. IEDM1987, USA: Washington, 1987: 485 – 488.

[16] Booske J H, Converse M C, Kory C L, *et al.* Accurate parametric modeling of folded waveguide circuits for millimeter-wave traveling wave tubes[J]. *IEEE Trans. Electron Devices*, 2005, **52**(5): 685 – 694.

[17] Shin Y M, So J K, Han S T, *et al.* Microfabrication of millimeter wave vacuum electron devices by two-step deep-etch x-ray lithography[J]. *Appl. Phys. Lett*, 2006, **88**: 16 – 19.

[18] Tucek J, Gallagher D, Kreischer K. A Compact, high power, 0.65 THz source[C]. IVEC2008, USA: Monterey, 2008: 16 – 17.

(上接 54 页)

[9] Graf A, Arndt M, Sauer M, *et al.* Review of micromachined thermopiles for infrared detection [J], *Measurement Science and Technology*, 2007, 18: R59 – R75.

[10] Chen Er-Zhu, Liang Ping-Zhi. Infrared microbolometer of lateral polysiliconp + p-n + junction based on standard CMOS process[J]. *J. infrared millim. waves*(陈二柱, 梁平治. 基于 CMOS 工艺的横向多晶硅 p^ + p^-n^ + 结红外微测辐射热计. 红外与毫米波学报), 2005, **24**(3): 227 – 230.

[11] Calaza C, Viarani N, Pedretty C, *et al.* An uncooled infrared focal plane array for low-cost applications fabricated with standard CMOS technology[J]. *Sensors and Actuators A*, 2006, 132: 129 – 138.